本科毕业设计（论文）答辩文件手册

题　　目：迈克尔逊干涉仪条纹分析特性与仿真

学 生 姓 名：

学　　号：

班　　级：

专　　业：

院 （系）：

指 导 教 师：

职　　称：

本科毕业设计(论文)文献综述

论文题目：迈克尔逊干涉仪条纹特性分析与仿真

文 献 综 述

1．前言

1883 年美国物理学家迈克尔逊和莫雷合作，以证明“以太”的存在而设计了世界上第一台用于精密测量的干涉仪——迈克尔逊干涉仪，它是在平板或薄膜干涉现象的基础上发展起来的[1]。迈克尔逊干涉仪在科学发展史上起了很大的作用，著名的迈克尔逊干涉实验否定了“以太”的存在。发现了真空中的光速为恒定值，为爱因斯坦的相对论奠定了基础。迈克尔逊用镉红光波长作为干涉仪光源来测量标准米尺的长度，建立了以光波长为基准的绝对长度标准。迈克尔逊还用该干涉仪测量出太阳系以外星球的大小。

通过对迈克尔逊干涉仪原理及干涉理论的研究分析，解释试验过程中出现密和粗而疏的条纹原因，并针对调节过程中常常出现的非标准干涉条纹的现象提出相应的解决方案。

迈克尔逊干涉仪，它是利用分振幅法产生双光束以实现干涉。通过调整该干涉仪，可以产生等厚干涉条纹，也可以产生等倾干涉条纹[2]。主要用于长度和折射率的测量，在近代物理和近代计量技术中，它在光谱线精细结构的研究和用光波标定标准米尺等实验中有着重要的应用

目前已经有几个著名厂家的成熟的干涉仪产品，覆盖了相当大的应用范围。但是干涉仪毕竟不是一个简单的工具，没有一定的理论基础难以正确使用，何况还有许多新的应用领域有待研究，需要更加深入的理论知识。等倾、等厚干涉原理是研究干涉技术的重要知识点之一，掌握等倾、等厚干涉原理及应用对进一步研究干涉测量技术有着重大的现实意义[3]。而这两种干涉条纹的应用也十分的广泛，等倾干涉条纹可以测量透明平板的厚度和折射率，等厚干涉条纹可以测量波长，薄膜厚度，液体折射率等等。

在国内外的相关研究中，虽然关于等倾干涉和等倾干涉都有相关的探讨，但是能将两者的异同点系统化地加以比较的并不多见。而且国内的文献中较少有将等倾干涉和等厚干涉基本原理与相关应用结合进行系统研究。

本文将结合在光学学习过程中的心得体会,依据波动光学的相关知识点，结合前人的探讨结果，从以下方面讨论了光的等倾干涉、等厚干涉及迈克尔逊干涉条纹非标准现象讨论:等倾、等厚干涉基本原理、计算方法、条纹特点，迈克尔逊干涉非标准条纹如何解决等。从而较深入的探讨了等倾、等厚干涉的本质。在此基础上希望能对大家更好地运用光学知识有所帮助。

2．主体

在 2015 年 4 月，乔亮等人对等倾、等厚干涉条纹实验用 MATLAB 进行了仿真实验。

两列相干光在某个点相互叠加，他们的合成光强分布为$I = I_1 + I_2 + 2\sqrt{I_1 I_2}\cos\delta$，式中$\delta$为两列光波的相位差。基于上述的理论，在 MATLAB 中设计以下仿真程序：

```
f = 0. 2 ;
lambda = 632. 8* 10^(-9)
d = 2. 5* 10^(-4) ;
theta = 0. 20 ;
rMax = f* tan(theta /2) ;
N = 501 ;
for i = 1 : N
x(i) = (i-1) * 2* rMax / (N-1) -rMax ;
for j = 1 : N
y(j) = (j-1) * 2*rMax / (N-1) -rMax ;
r(i, j) = sqrt(x(i) ^2 + y(j) ^2) ;
delta(i, j) =2* d / sqrt(1 +r(i, j) ^2 /f^2) ;
Phi(i, j) =2*pi*delta(i, j) / lambda ;
B (i, j) = 4* cos(Phi(i, j) /2) ^2 ;
end
end
NCLevels = 255 ; Br = (B /4. 0) * NCLevels ;
figure( 1) ; image(x, y, Br) ;
colormap(gray(NCLevels) ) ;
axis square ;
```

图 1 仿真程序

如图2所示为利用MATLAB模拟入射波波长为 632.8nm的等倾干涉条纹图样，程序中可以通过改变空气薄层的厚度和入射倾角得到不同的干涉条纹图样。在实验操作中，得到此同心圆环状的干涉条纹后，继续微调反射镜M_2使得M_2'与M_1产生微小的倾角(图5)，便可以实现图3的等厚干涉条纹。

图 2 等倾干涉条纹仿真图

图 3 等厚干涉条纹仿真图

在 2019 年 9 月杨文虎等人对迈克尔逊干涉实验的非标准干涉现象进行了讨论及提出了解决的方法[4]。

光路原理图如图 4，理论分析如图 5 所示：光源 S 与干涉轴线垂直，经半透镜 G_1 和补偿镜 G_2 分成两束光，由平面镜 M_2 通过半透半反镜 G_1 成虚像 M_2'。故可认为两束相干光线是由 M_1 和 M_2'反射来的。也可视为由虚光源 S_1 和 S_2 发出其间距为 $2d$(d 为 M_1 和 M_2'之间的距离)。ϕ 为光从 S_1 点射向中心 S'点下射向 A 点的夹角。

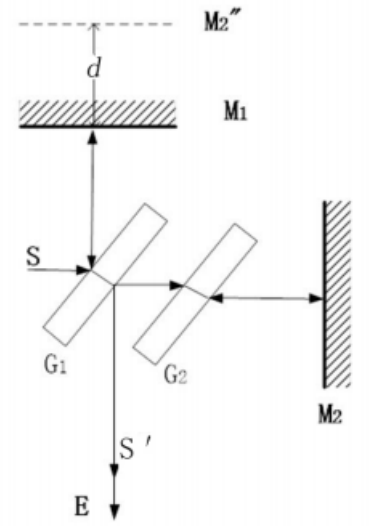

图 4 迈克尔逊干涉仪的光路原理图

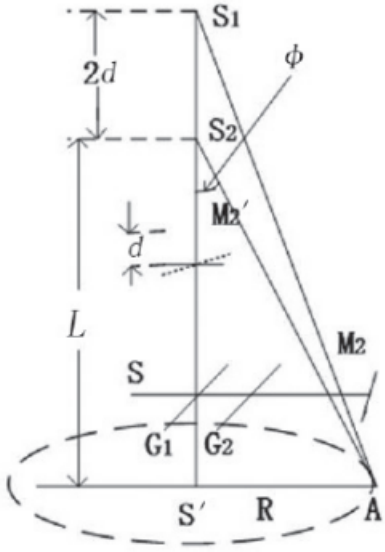

图 5 非定域等倾干涉条纹产生原图

(1)形成干涉的圆环现象

由S_1和S_2 到屏E上任一点A两光的光程差为：

$$\Delta d = S_1A - S_2A \qquad \text{公式（1）}$$

由于$d<<L$，且ϕ极小，可以近似得出：

$$\Delta d = 2d\cos\theta \approx 2d(1-\tfrac{1}{2}\theta^2) \qquad \text{公式（2）}$$

当$\Delta d = 2d\cos\theta = K\lambda$（$K \in N$），干涉条纹中心为明纹；

$\Delta d = 2d\cos\theta = (2K+1)\tfrac{1}{2}(K \in N)$，干涉条纹中心为暗纹。

则可在观察屏的中间观察到明暗相间的标准同心圆环。

(2)条纹外缩与内缩现象

在任意K级条纹，当$\Delta d = K\lambda$时，为明纹。

由于$2d\cos\theta = K\lambda$时为明纹，则其到中心S′的半径$R = L\tan\theta$。

移动平面镜M_1，当M_1与M_2'之间的间距d减小时，当第K级明明纹$K\lambda$不变，$\cos\theta$变大。

由于θ的角度很小，$\cos\theta$变大，则角度变小θ。

由于θ的角度很小，θ角度变小，$\tan\theta$变大，则有R半径增大。

当M_1与M_2'之间的间距d减小时，第K级的干涉条纹向圆心内移，使条纹由外往里收缩变粗而疏。

(1)当两平面镜M_1与M_2垂直则$M_1//M_2''$（如图4所示），而入射光源不与干涉仪轴线垂直，干涉环的中心将偏离屏中心(如图6所示)。由实验图像a →实验图像e，随着M_1与M_2'光程差d减小，干涉条纹的中心将渐次远离中心，观察到的干涉条纹为弧线甚至近乎为一条直线。由图像比对分析得出结论：入射光源不与干涉仪轴线垂直时，光差M_1与M_2光程差d越小，干涉圆心就越偏，越不易观察。

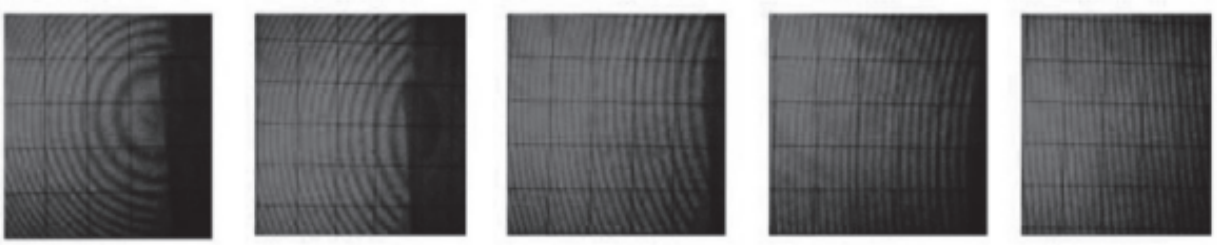

a动镜读数为 45.94960　b动镜读数为 47.92040　c动镜读数为 48.94040　d动镜读数为 49.93041　e动镜读数为 50.92042

图 6 入射光偏离干涉轴

(2)当两平面镜 M_1 与 M_2 不严格垂直，则 M_1 与 M_2''（图 4）则不平行。

如 M_1 与 M_2'夹角接近平行时，光源 S 与干涉轴线垂直。如图 7 所示，由实验图像中平镜 M_1 与 M_2'距离 d，由图像 a→图像 b→图像 c 减小，再由图像 c→图像 d→图像 e 增大；如 M_1 与 M_2 夹角较大时，则找不到干涉条纹。因此由图像比对分析得出结论：其光程差越小，图像越混浊不清晰，越难观察。

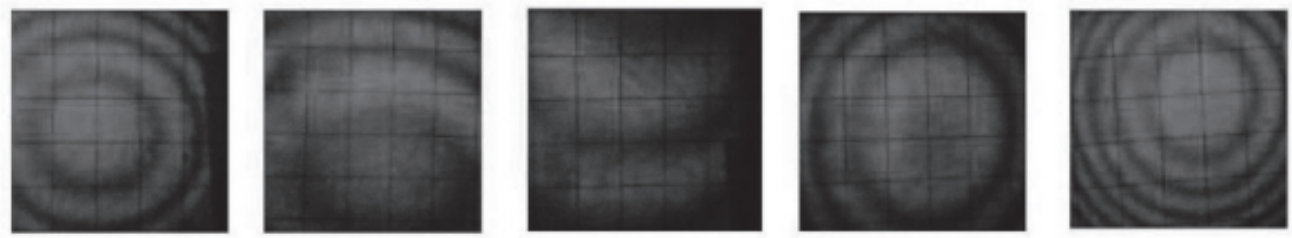

a动镜读数为 52.93000　b动镜读数为 51.92989　c动镜读数为 50.93033　d动镜读数为 49.92918　e动镜读数为 48.92992

图 7　M_1 与 M_2''有夹角的情况下，光程差在 0 左右。

3．总结

我认为目前的焦点是如何利用 MATLAB 仿真迈克尔逊干涉条纹的各种条纹，学者们也对其问题进行了分析。对我来说乔亮等人对等倾干涉条纹，等厚干涉条纹的仿真研究是非常有必要的，这能弥补我国对迈克尔逊干涉条纹研究的空缺，教会我国学者怎么用代码对条纹进行分析与调整。但在搜集文献的过程中我还发现，在从等倾，等厚干涉条纹的定位出发，观察不同条纹的问题以及解决方法的途径上，在这方面应该具有更具体的措施[5]。比如，我们还可以对杨氏双缝干涉实验仿真，牛顿环干涉实验仿真等等，这就能更加的对迈克尔逊干涉条纹实验进行研究和实验，能让我们更加快速全面的理解其条纹。

学习了迈克尔逊干涉仪，我们就应该将其运用在实践中。在利用迈克尔逊干涉仪来测量液体折射率时，我们首先得先了解到折射率是物质的一个重要光学参数。目前我认为利用迈克尔逊干涉仪测量液体折射率最主要的是在光路中设置一个盛待测液体的装置，这是实验的关键[6]。韦仙等人就进行了这样的实验，他们设计的方案能扩展迈克尔干涉仪的应用，原理也比较的简单，便于我们大学生理解，实用可行，比较适合利用于实验教学。但是我认为他们的实验也还有不足，他们只对其一种液体进行了测量，这没有对比性的，而且做的实验次数比较少，误差也比较大。这个实验如果多对两种不同液体进行实验那就能弥补其中的不足。

利用迈克尔逊干涉仪测量金属丝的杨氏模量也是一种实践应用，刘金秋等人进行了实验。他们的实验比传统的杨氏模量仪的测量方法比较起来是很方便简单的，而且得出的杨氏模量精度更高，误差也比较小，适用范围也广泛，这对测量杨氏模量有很重大的意义，促进了我国对杨氏模量的研究[7]。我认为他们的这种方法就应该大力的推动，作为大学生我们就应该多动脑思考问题，多动手解决不会的问题。

学习了迈克尔逊干涉仪就应该知道测量波长的不等间隔条纹计数法，这是教学当中的重点，是必做的实验项目。艾德智对不等间隔条纹计数法进行了探讨[8]。因为目前采用的条纹计数方法，实验者的用眼强度很高，对眼睛的承受力是一种挑战。针对这个问题，他们提出采用条纹自动计数装置来改善，这种改进方法是需要通过电路来完成，这种方法的精度就很高，能有效的缓解实验者的视觉疲劳，减少对眼睛的伤害[9]。但我认为电路的调试过程比较繁琐，对实验环境要求很高，且对电路元器件的可靠性及电路的稳定性要求也比较高，一旦出现差错，就会导致波长测量的失败[10]。但总体来说我十分认可他们的这种方法，这是一种很高效的方法。

4．参考文献

[1]Ghoname Amr O, Hassanien Ahmed E, Chow Edmond Lynford L, Gon Songbin. Highly linear lithium niobate Michelson interferometer modultors assisted by spiral Bragg grating reflectors. [J]. Optics express, 2022, 30(22).

[2]Shao Min, Cao Zhongwei, Gao Hong, Hao Minru,Qiao Xueguang. Large measurement-range and lowtemperature cross-sensitivity optical fiber curvature sensor based on Michelson interferometer[J]. Optical Fiber Technology, 2022, 72.

[3]Song Ruogu, Sun Jialiang, Wang Jinyu, Li Xinyu, Liu Yufei, Yue Wencheng, Cai Yan,Wang Shuxiao, YuMingbin. High-speed compact folded Michelson interferometer modulator. [J]. Optics express, 2022, 30(13).

[4]杨文虎,赖学辉,李永强,张海康,郑明军,莫竣成.迈克尔逊干涉实验的非标准干涉现象及解决的方法[J].中国现代教育装备,2019,(21):91-92+96.

[5]乔亮，羊富贵，夏忠朝，江琳沁. 基于 Matlab 的迈克尔逊干涉实验仿真[J]. 大学物理实验，2015,28(02):93-95.DOI:10.14139/j.cnki.cn22-1228.2015.02.026.

[6]韦仙，冯中营，刘晓菲, 曾霄. 基于 Matlab 的迈克尔逊干涉仪测液体折射率仿真研究[J]. 大学物理实验，2018,31(02):92-95.DOI:10.14139/j.cnki.cn22-1228.2018.02.024.

[7]刘金秋，郑运强，赵珊珊，智春艳，赵朝军，邱文旭.基于迈克尔逊干涉仪测量金属丝的杨氏模量[J]. 科技风，2020(21):71.DOI:10.19392/j.cnki.1671-7341.202021060.

[8]艾德智，王哲婕，薛江蓉. 迈克尔逊干涉仪测波长的不等间隔条纹计数法的探讨[J]. 大学物理实验，2018,31(05):9-11.DOI:10.14139/j.cnki.cn22-1228.2018.05.003.

[9]王哲婕，艾德智，陆苑英，孙健，薛江蓉. 探究不同条纹计数法对波长测量精度的影响[J]. 大学物理实，2019,32(04):9-12.DOI:10.14139/j.cnki.cn22-1228.2019.04.003.

[10]张定梅，蒋再富，孙宪钢. 基于迈克尔逊干涉仪测金属线胀系数[J]. 实验室科学，2018，21(04):20-22.

5．指导教师意见

【指导教师第一次评阅意见】

按附件批注修改

【指导教师第二次评阅通过】

罗天程同学通过对迈克尔逊干涉仪相关文献的阅读，对该领域有了一定的理论总结。毕业设计前期态度端正，对文献的调研和理解基本准确，文献综述语句通顺，格式正 确，达到毕业设计文献综述的要求。

指导教师（签字）： 

2023 年 02 月 06 日

成都工業學院
Chengdu Technological University

本科毕业设计(论文)英文翻译

论文题目：迈克尔逊干涉仪条纹特性分析与仿真

学 生 姓 名：	罗天程
学　　号：	1903031127
班　　级：	19 电科 1 班
专　　业：	电子科学与技术
院　（系）：	电子工程学院
指 导 教 师：	廖无瑕

二零二三年二月二十七日

一、英文原文

起止页码：1～9

出版日期（期刊号）：2018/09/06

刊物名称（出版单位）：Proceedings for ICSO 2018

Study of the coherent perturbation of a Michelson interferometer due to the return from a scattering surface

Vitalii Khodnevych, Sibilla Di Pace, Jean-Yves Vinet, Nicoleta Dinu-Jaeger and Michel Lintz
ARTEMIS, Universite and Observatoire de la Cote d'Azur, CNRS, Nice, France

ABSTRACT

We describe a setup based on Michelson interferometry for coherent measurements of the backscattered light from a low roughness optical surface under test. Special data processing was developed for the extraction of the useful signal from the various stray contributions to the coherent signal. We achieve coherent detection of light scattered by a mirror down to -130 dB in optical power. We characterize the dependence of the backscattered light with spot position and incidence angle. Results of cross-polarization scattering coherent measurements and preliminary results of dust deposition experiment are presented here. This work represents the first step in the experimental evaluation of the coherent perturbation induced by the scattered light in the space gravitational wave detector of the LISA mission.

Keywords: LISA mission; Scattered light; Michelson interferometer

1. INTRODUCTION

The Laser Interferometer Space Antenna (LISA) is a space-based gravitational wave observatory[1] now in Phase A. It is represented by a triangular constellation of three identical satellites, each satellite containing two gravitational reference sensors (e.g. test masses) at the end of each arm. The measurement of length variation between the two test - masses, variation driven by gravitational waves but also by various noise sources, is provided by heterodyne interferometry.

Any source of coherent scattered light can perturb the interferometric measurement since it can give rise to a significant noise during the heterodyne phase measurement at a level of one or several micro-radians.

Before evolving strategies to mitigate scattered light in the LISA instrument, and since the backscattered light in the telescope can affect the long arm (2.5 millions of km) length measurement, a good understanding of the perturbation of heterodyne interferometry by scattered light has to be achieved prior to mission launch.

2. SETUP

As a first step, we have implemented a setup for the coherent measurement of backscattered light (see fig.1). The setup is split in two parts: a fibered one, containing the laser source and a fibered Michelson interferometer, and a free space one with optics designed to illuminate the sample under test with a collimated beam and to collect the backscattered light. A lock-in detection is used to drive a phase modulation applied to the beam and to demodulate the fringe signals.

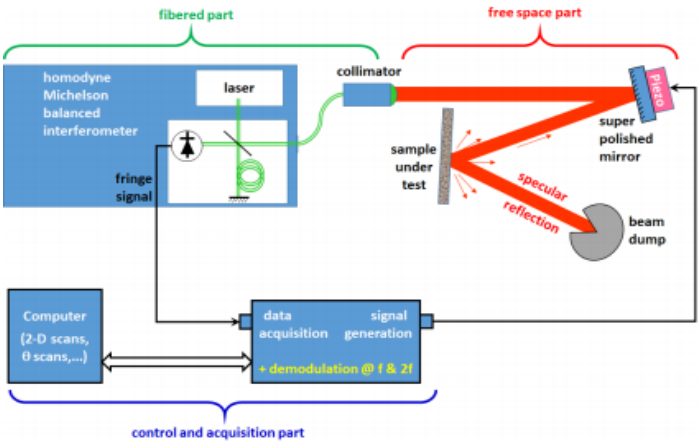

Figure 1. Block diagram of the coherent back-scattering measurement set-up

The detailed schematics of the setup is shown in figure 2. The basis of this setup is a Fibered Michelson interferometer. We use a narrow linewidth Orion RIO infrared laser diode of 1.542μm wavelength and 10.2mW power. An optical circulator, inserted between the laser source and the beam splitter, prevents the laser from receiving the fraction of the light which is rejected by the Michelson interferometer and could otherwise cause amplitude and frequency modulation in the laser. Instead, the rejected beam is sent to a second photodiode (PD_2), to increase the gain and precision of the measurements. Then the light is divided by the fibered 50/50 beam splitter and follows the two arms of the interferometer. Arm I is fully fibered, with a fibered 100% reflector and, if a scan of the optical phase difference is useful, a thermal ramp can be applied. Arm II is partially fibered, up to a collimator, which emits a collimated beam for the free space part. All optical fibers are polarization maintaining.

The collimated beam in the free space propagates to a super polished mirror with a piezo actuator for rapid modulation of the optical phase. The piezo is powered by a 2 kHz sine from the internal signal generator of the lock-in amplifier. From the piezo mirror, the collimated, phase modulated beam propagates to the sample under test, its backscattering being the aim of our measurements. The backscattered light which is recoupled into the fiber interferes with the beam from Arm I. A beam dump[2] is placed in such way to attenuate efficiently the specularly reflected beam from the sample. In the presence of the backscattering, the interference between ARM I and ARM II beams gives rise to a modulation in the photodiode signals. The modulated signal are amplified, and then demodulated by a lock-in amplifier.

As will be shown in the following,the scattered light has a speckle behavior as a function of the incidence angle, and it is possible to adjust the position and the incident angle at the beam dump to minimize its backscattering. The beam dump is made from two black HOYA RT-830 glass plates polished by Coastline Optics. The two absorbing glass plates are placed, parallel to each other, so that the lasers beam bounces a number of times and is attenuated. The minimized backscattering, which we measure from this beam dump is - 130.9±0.9 dB in optical power. To separate the contribution of the beam dump from other contributions to backscattering, we modulate the position of the beam dump at the frequency of 1 Hz, and identify the corresponding contribution in the fringe signal. When the incidence at the beam dump is well adjusted, we switch the 1 Hz signal to modulate the sample position. With properly adjusted amplitude we completely discriminate the contribution of the backscattering of the sample against other contributions (see below). To make 2D maps of the backscattering amplitude, we use a 2D translation stage controlled from a PC to move the sample parallel to its surface. For angular study of scattered light,we use a Picomotor rotational stage (New Focus 8821) instead of the 2D stage.

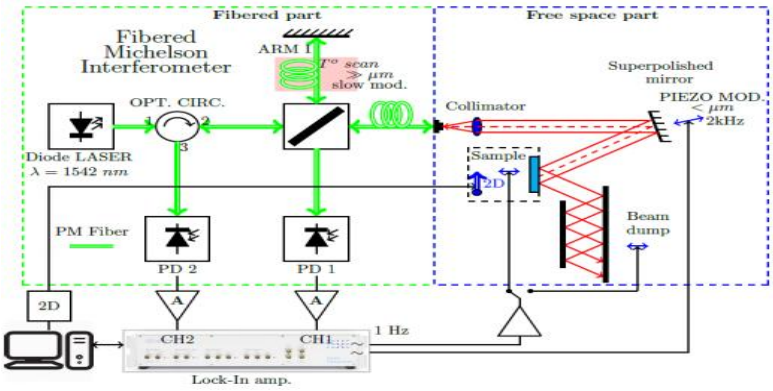

Figure 2. Coherent backscattering measurement setup. Green: optical fibers. Red: freespace beams. Dashed red: backscattered light from the samp

The same interferometric set-up is used for the measurement of coherent backscattering from dust deposition (see Results section and Fig. 9). A controlled deposition of a given size and number of dust particles on the mirror is obtained by using a spray system. A camera and a white light illuminating LED are placed in front of the sample. Using image processing of the camera images, the information related to the number of particles on the sample and it is subsequently correlated with the measured interferometric signal.

3. DATA PROCESSING

Ideally, after recombination at the 50/50 beam splitter, the backscattered fraction of light from the sample surface, with an amplitude of $A = \sqrt{I_L/4}\sqrt{b_s}\exp(i\phi_\Pi, s)$, interferes, with the light of amplitude $A = \sqrt{I_L/4}\exp(i\phi_I)$. At the PD_1 (resp.PD_2) output ports of the interferometer, the interference signal is $I = I_L/2 \times \sqrt{b_s}\cos(\Delta\phi_s)[resp.is - I_L/2 \times \sqrt{b_s}\cos(\Delta\phi_s)]$,In this expression I_L

is the laser intensity, $\Delta\phi_s = \phi_{\Pi,s} - \phi_I$ is the difference of the propagation phase between arm II (up to the sample), including the 2 kHz modulation of the piezo actuator,and the arm I, including a possible thermal ramp. Then extracting the backscattered power fraction b_s by demodulation looks trivial.

However, the processing of demodulated signals is complicate because multiple contributions from different backscattering sources(e.g.fibers, fiber connectors, collimator, piezo mirror, beam dump, and sample)are presented in the measured signal. First, one could consider separately the three sources located before the piezo mirror, from which backscattering signal should not be modulated, and discard them. But the acoustic crosstalk between the fibered part and the piezo actuator is not negligible, as we clearly observe the corresponding contribution demodulated signal. Other contributions to backscattering come from the modulated mirror and from the beam dump. Therefore,the total fringe signal at PD_1 has to be written as following.

$$I = \frac{I_L}{2}\left(\sum_I \sqrt{b_i}\cos(\Delta\phi_i) + \sqrt{b_s}\cos(\Delta\phi_s)\right) \qquad (1)$$

where all stray contributions to backscattering (power ratio and phase ϕ) are under the sum sign.Demodulation is done at the first harmonic (frequency 2 kHz) with a bandwidth of 6 Hz (8th order). After demodulation of the signal using the lock-in amplifier,we get 224 times per second, in-phase X and quadrature Y components. The combination we need is:

$$R = \cos(\Theta)\times X + \sin(\Theta)\times Y \qquad (2)$$

where Θ is the phase of the fringe signal modulation with respect to the voltage applied to the piezo actuator. It differs from zero due partly to the electronic signal propagation delay and mainly to the hysteresis in the piezo actuator. As Θ does not change during data taking we first determine the value of Θ in conditions where the signal is large. Later we use this value to determine R from eq.2, and exploit the time series of R, particularly the dependance of R on the thermal drift of the fibered path length and/or on the modulations we apply to the position of the sample. Then the demodulated signal of the measured signal at the first and second harmonics of piezo mirror modulation frequency (2 kHz) will be:

$$R_1 = I_l\left(\Sigma_i\sqrt{b_i}J_1(2\pi\delta_{PMi})\cos(\phi_i) + \sqrt{b_s}J_1(2\pi\delta_{PM})\cos(\phi_s)\right) \qquad R_2 = I_L(\Sigma_i$$

where $J1$ is Bessel function of first order and PM is the modulation depth of the piezo mirror (note that for each component modulation depth can be different). Separation of the contributions from all backscattering sources is a difficult and unnecessary task. What we need is to give a specific signature to the $\sqrt{b_s}$ contribution, to identify and record it with the highest precision. Using Fast Fourier Transform (FFT) we can easily extract all harmonics of the modulated signal from R_1. When modulation of the sample is applied, we have an additional term in phase ϕ_S for sample and beam dump components:

$$R_1 = I_L(\sum\sqrt{b_i}J_1(2\pi\delta_{PM})\cos(\phi_i)+\sqrt{b_s}J_1(2\pi\delta_{PM})\cos(\phi_s+\delta_1\cos(\omega_s t)) \\ +\sqrt{b_{BD}}J_1(2\pi\delta_{PM})\cos(\phi_{BD}+2\delta_1\cos(\omega_s t+\phi_0))) \quad (4)$$

Similar for the second harmonic. Here δ_1 is the slow frequency modulation depth and $\phi_0 \approx 1$ is a propagation delay (sample-beam dump-sample). The factor two in front of the modulation term considers that the backscattered light from the beam dump is twice modulated. In fig. 3 is presented the FFT of R_1 in different measurement conditions, but for the same scattering point. In red is the FFT of R_1 when 1 Hz modulation is applied to the sample. At very low frequency (below 1 Hz) are spectral components of the parasite backscattering contributions. They are not modulated, so they contribute only on frequencies <1 Hz, due to thermal drifts. At higher frequencies modulation harmonics at 1 Hz of useful signal mixed with the beam dump backscattering contribution. It's interesting to recall that functions of type $\cos(\phi + \delta\sin(\omega_s t))$ can be presented as series:

$$J_0(\delta)\cos(\delta)+2\sum\nolimits_n J_{2n}(\delta)\cos(2n\omega_s t)\cos(\phi)-2\sum\nolimits_n J_{2n-1}(\delta)\cos((2n-1)\omega_s t)\sin(\phi) \quad (5)$$

So, the distribution of the power between harmonics is given by the Bessel function of the first kind. Argument of this function is the modulation depth δ. By adjusting the δ, we can redistribute the power in the spectrum in a desired way. This property is useful, as a spectrum (5) has slow (thermal) component multiplied on J_0. If we adjust δ, so that $J_{0\,(6)} = 0$, then we will have useful signal separated in frequency from parasite ones. So, for this procedure, it is crucial to adjust the modulation depth of the sample in a way to reach the zero of Bessel function of zero order.

The Figure 3 shows also the FFT of R_1 when slow modulation is not applied (green color). In this case, the contributions of backscattering are not separable, and any precise measurements are not possible. In blue in the same figure is shown the case when neither slow nor fast modulation is applied to the setup. So, this displays the contributions to the noise floor from the laser power noise and electronic noise of the detection system.

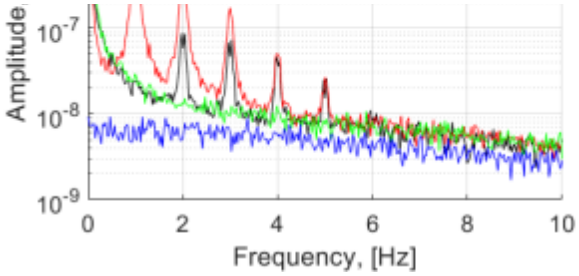

Figure 3. FFT of *R1* when slow (1 Hz) modulation is applied to the beam dump (black), and the case without slow modulation (green). For the sample modulation (red) we had adjusted the voltage to reach the condition

$J0_{(6)}$ = 0.The case when neither the fast,nor the slow is applied gives electronics plus laser noise level (blue).

4. RESULTS

Speckle behavior of scattered light is observable when the sample is moved parallel to its optical surface, using the setup shown in Fig.2. The correlation length under the translation of the sample is compatible with the beam waist (see fig. 4). In this figure is shown measured backscattering fraction in amplitude,when we translate the sample. The beam shape shown in black is a Gaussian intensity profile with the size of the collimated beam (ω_0 =1.71 mm).

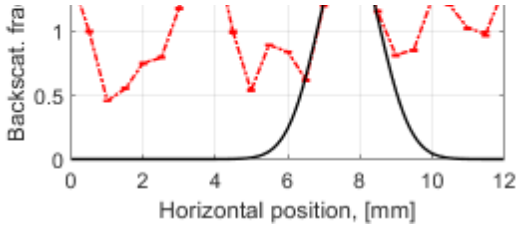

Figure 4. Profile of backscattered light from a moderately scattering target.Black curve (arbitrary units): plotted for comparison,a gaussian beam profile of the same gaussian beam size (ω_0 =1.71 mm) as the incident beam.

For the sample under test, a 1-inch "IR mirror" from Edmund Optics (ref. 47113) has been used. It has RMS roughness less than 175A. This value is large,however it is small enough that scattering is still in the "small roughness" regime.The mirror roughness is probed by a collimated beam with gaussian size ω_0 =1.71mm obtained from an 18 mm focal length collimator. The 2D translation of the sample is carried out by the Newport translation stage with a step 0.5mm over a distance of 12mm. The beam in the free space part of the setup has a beam divergence angle of 0.58 mrad.

The 2D maps in Figure 5 show rapid changes with the incidence angle at the sample. Because the change of incidence is small compared to the beam divergence, one can follow the correlation between successive scattering maps.

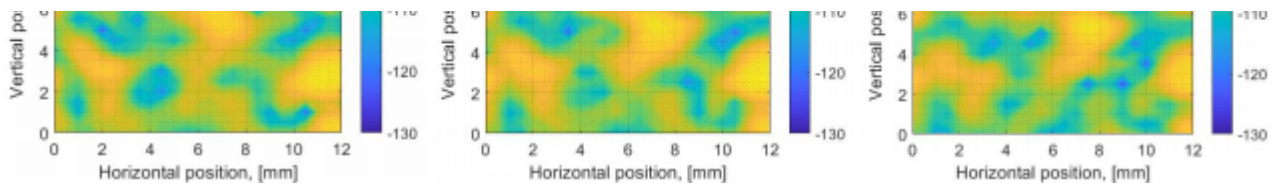

Figure 5. 2D maps of the backscattered power (in dB) of the same scanning area with slightly different incidence angle (20 μrad steps).

5. CONCLUSIONS

We have developed a setup and data processing for the measurements of the backscattered light from an imperfect surface with a view at the scattered light issues in the LISA mission. We have studied scattered light from an IR mirror with intermediate roughness (less than 175 *A* rms roughness). We have observed, in the coherent backscattering amplitude, speckle-type dependence with spot position and incidence angle, as can be expected from the stochastic nature of the roughness profile. We had found that size of speckle grain corresponds to the size of the beam. Crossed polarization of backscattered light is present and it is not negligible. These observations will be improved, particularly by measuring the dependence with large incidence angle changes, for comparison with models based on the measured roughness profile, and with models based on the measurement of the bi-directionnal reflectance distribution function (BRDF) of the samples.

Preliminary observation was made of the correlation between the coherent backscattering amplitude and the number of dust particles. As preventing the deposition of dust during the assembly and launch phases of the LISA mission will be difficult, this study will be improved and extended. White light images will be used to retrieve, not only the number of particles, but also their size and position, and to model the coherent scattering from the observed dust distribution.